7-2014

Finite element modeling of long-term phosphorus leaching through macropores in the Ozark ecoregion

Ryan P. Freiberger
University of Nebraska-Lincoln

Derek M. Heeren
University of Nebraska-Lincoln, derek.heeren@unl.edu

Garey A. Fox
Oklahoma State University, gafox2@ncsu.edu

Chad J. Penn
Oklahoma State University

Dean E. Eisenhauer
University of Nebraska-Lincoln, deisenhauer1@unl.edu

2950 Niles Road, St. Joseph, MI 49085-9659, USA
269.429.0300 fax 269.429.3852 hq@asabe.org www.asabe.org

CSBE | SCGAB

An ASABE – CSBE/ASABE Joint Meeting Presentation

Paper Number: 141897543

Finite element modeling of long-term phosphorus leaching through macropores in the Ozark ecoregion

Ryan P. Freiberger[1], Derek M. Heeren[1], Garey A. Fox[2], Chad J. Penn[3], and Dean E. Eisenhauer[1]

[1] Biological Systems Engineering, University of Nebraska - Lincoln, Chase Hall, Lincoln, NE, 68583

[2] Biosystems and Agricultural Engineering, Oklahoma State University, Agricultural Hall, Stillwater, OK, 74078

[3] Plant and Soil Sciences, Oklahoma State University, Agricultural Hall, Stillwater, OK, 74078

Written for presentation at the

2014 ASABE and CSBE/SCGAB Annual International Meeting

Sponsored by ASABE

Montreal, Quebec Canada

July 13 – 16, 2014

Abstract. Phosphorus (P) is a critical nutrient for plant growth in agriculture, but is also responsible for surface water enrichment that leads to toxic algal growth. While P loading to surface waters has traditionally been thought to occur from surface runoff, contributions from subsurface transport can also be significant. While P transport through many soil types is well-documented, the presence of highly conductive gravel outcrops and macropore networks can have a significant, yet poorly-documented effect on P movement to the aquifer. Floodplain soils in the Ozark ecoregion generally contain coarse chert gravel layers that exhibit macropore behavior. Previous research has evaluated short-term P transport in plot trials ranging from 1 m^2 to 100 m^2 across many Ozark ecoregion floodplain sites. Traditional methods of estimating P loading and soil saturation do not account for macropore flow and likely underestimate P transport to the water table. To address this concern, long-term P modeling was performed in HYDRUS-2D/3D using data collected from short-term plot experiments. Calibration was performed using single- and dual-porosity models with both homogeneous and heterogeneous gravel profiles. The dual-porosity model with heterogeneous hydraulic conductivity best matched experimental data, although the dual-porosity model with homogenous soil layers also performed well. Long-term P transport to a 3 m-deep water table was simulated using 9 years of both daily and 5 minute rainfall data with a P flux consistent with yearly poultry litter applications. Long-term simulations with 5 minute rainfall data found that 113 kg ha^{-1} reached the water table over 9 years, or 21% of P applied.

Keywords. *dual-porosity, finite element, infiltration, macropore, phosphorus, subsurface transport.*

Introduction

Phosphorus is an important nutrient for crop growth and development, but overloading of freshwater systems with phosphorus can induce significant algae growth. Algal blooms and cyanobacteria outbreaks contribute to hypoxic waters and fish kills, as well as reduce the quality of water for consumption and recreational use (Lopez et. al., 2008). Phosphorous (P) transport has been assumed to take place primarily in surface runoff, although a growing collection of research indicates that subsurface P transport can be significant (Osborne and Kovacic, 1993; Cooper et al., 1995; Gburek et al., 2005; Fuchs et al., 2009). Large scale streambank storage of P-laden stream water during high flow discharges can result in P-laden groundwater in alluvial aquifers which migrates back to the stream during baseflow conditions (Heeren et al., 2011). These subsurface P transport rates in Ozark floodplains have been shown to be comparable to surface runoff P transport rates (Mittelstet et al., 2011). In many gravelly floodplains, gravel outcrops and macropores are present resulting in high infiltration rates, some of which are reported to be on the order of 10 to 100 cm hr^{-1} (Heeren et al., 2014; Heeren et al., 2013). It has been shown that in porous media with heterogeneous flow properties, the majority of the flow can occur in small preferential flow paths (Gotovac et al., 2009; Najm et al., 2010). Djodjic et al. (2004) performed experiments on P leaching through undisturbed soil columns, and stressed the need to consider larger-scale leaching processes due to soil heterogeneity.

Accurately modeling macropores is a complicated process. Possibly the best available means of modeling macroporosity in a soil is through the use of a multi-domain system (Beven and Germann, 1982; Šimůnek and van Genuchten, 2008). Multi-domain models split the soil profile into a fracture (macropore) domain and a matrix domain. Such models account for high flows and solute transport rates that are linked to macroporosity in soils. Multi-domain models express physical transport in several ways. Mobile-immobile (MIM) models define water and solute flow through the macropore space, with solute transport also occurring between the immobile and mobile phases through molecular diffusion (Figure 1a). Dual-porosity models build upon this further by allowing both water flow and solute transport (through advection as well as diffusion) to occur between the mobile and immobile phases (Figure 1b). Dual-permeability models are somewhat different, where mobile and immobile phases are replaced with “fast” and “slow” zones, respectively (Figure 1c). Both zones allow for water and solute transport, but do so at different rates. A last model combines dual-permeability and MIM phases, so that solute transport can also enter an immobile zone and is removed from transport (Figure 1d). State-of-the-art modeling programs, such as HYDRUS-1D or HYDRUS-2D/3D, offer these models to allow for maximum flexibility when modeling complex subsurface systems.

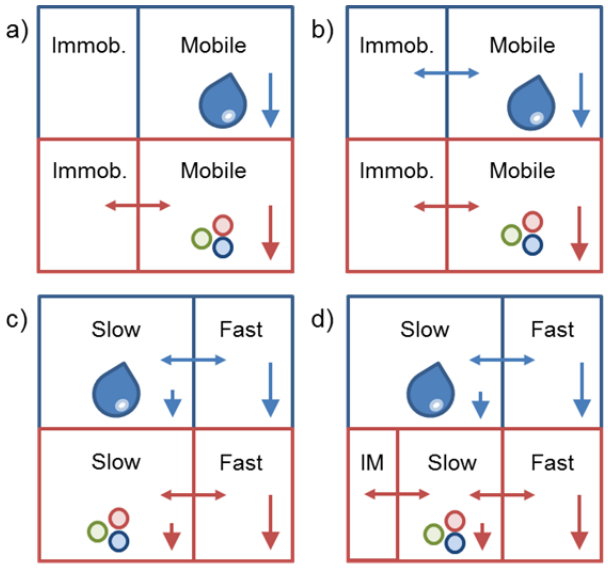

Figure 1. Conceptual models for macroporosity: (a) mobile-immobile, (b) dual-porosity, (c) dual-permeability, and (d) dual-permeability with a solute immobile zone. Adapted from Šimůnek and van Genuchten (2008).

Previous research has used multi-domain numerical models to model contaminant transport. Jarvis et al. (1999) used the dual-porosity MACRO model to simulate colloidal particle transport in silty clay loam soils in Sweden. Larsson et al. (2007) simulated P losses to tile drains in Swedish clay soils using the ICECREAM model. However, neither study evaluated extremely heterogeneous soil profiles. Furthermore, limited research has been done to evaluate P transport using HYDRUS-2D/3D or using soil profiles developed with electrical resistivity mapping.

Methods

Barren Fork Creek Field Site

Plot scale infiltration experiments were performed at the Barren Fork Creek floodplain site (Heeren et al., 2013), which was located in the Ozark region of northeastern Oklahoma, which is characterized by karst topography, including caves, springs, sink holes, and losing streams. The erosion of carbonate bedrock (primarily limestone) by slightly acidic water has left a large residuum of chert gravel in Ozark soils, with floodplains generally consisting of coarse chert gravel overlain by a mantle of gravelly loam or silt loam (Figure 2). Topsoil depth in the floodplains ranged from 1 to 300 cm in the Oklahoma Ozarks, and generally increased with increasing stream order. Common soil series include Elsah (frequently flooded, 0-3% slopes) in floodplains; Healing (occasionally flooded, 0-1% slopes) and Razort (occasionally flooded, 0-3% slopes) in floodplains and low stream terraces; Britwater (0-8 % slopes) on high stream terraces; and Clarksville (1-50%) on bluffs.

At the Barren Fork Creek site, located five miles east of Tahlequah, Oklahoma (latitude: 35.90°, longitude: -94.85°) and just downstream of the Eldon U.S. Geological Survey (USGS) gage station (07197000), soils were Razort gravelly loam. The silt loam layer was from 30 to 200 cm thick, and the chert gravel layer, ranging from 3 to 5 m, extended down to limestone bedrock. The gravel subsoil, classified as coarse gravel based on the Wentworth (1922) scale, consists of approximately 80% (by mass) of particle diameters greater than 2.0 mm, with an average particle size (d_{50}) of 13 mm (Fuchs et al., 2009). Estimates of hydraulic conductivity for the gravel subsoil range between 140 and 230 m d^{-1} based on falling-head trench tests (Fuchs et al., 2009). The gravel layer itself is a complex alluvial deposit (Figure 2) that includes both clean gravel lenses associated with rapid flow and transport (Fox et al., 2011) as well as layers of fine gravel that can cause lateral flow in the silt loam and subsequent seepage erosion (Correll et al., 2013). The anisotropic horizontal layering results in a propensity for lateral flow.

Figure 2. Streambank at the Barren Fork Creek field site including the bank profile (left) and a seepage undercut (right). Note the sloughed material in the bottom of each picture from recent bank failures. These complex alluvial deposits include both clean gravel lenses associated with rapid flow and transport (left) as well as fine gravel lenses that can cause lateral flow and seepage erosion.

The berm infiltration method (Heeren et al., 2014) was used to confine water and solutes at multiple infiltration plots (1 by 1 m to 10 m by 10 m) within the Barren Fork floodplain. A constant head of water and constant solute concentrations were maintained within the plots. Chloride (Cl^-) was used as a conservative (nonsorbing) tracer. Target tracer concentrations were 100 to 200 mg L^{-1} KCl (correlating to 48 to 95 mg L^{-1} Cl^-), depending on background EC levels. The P (highly sorbing) concentrations of approximately 3 mg L^{-1}(corresponding to 10 mg L^{-1} as phosphate) were used to represent poultry litter application rates (typically used as a fertilizer source in the Ozark ecoregion) in the range of 2 to 8 Mg ha^{-1} (1 to 3 ton $acre^{-1}$). The P concentrations were achieved by adding phosphoric acid (H_3PO_4), which deprotonated to $H_2PO_4^-$ and HPO_4^{2-} in the slightly acidic solution. Observation wells were installed near the plots in order to collect water samples to document solute

breakthrough curves. The infiltration data have been presented in Heeren et al. (2013), and the transport data in Heeren (2012). This research used HYDRUS to simulate the 1x1α infiltration plot at the Barren Fork Creek site.

Development of HYDRUS Model

The model was developed in HYDRUS using parameters established from previous research at multiple sites within the Ozark ecoregion, including the Barren Fork site. A 2-D slice of a soil profile was generated to match electrical resistivity imaging (ERI) data found by Miller et al. (2014) for the Barren Fork 1x1α site. The profile was divided into four distinct soil layers: a 1.33-m topsoil layer identified by Heeren (2012) and three subsurface gravel layers identified using ERI data (Figure 3). Values for van Genuchten parameters and soil material properties for the soil layers were estimated using the Rosetta Lite (v. 1.1) module embedded in HYDRUS. Gravel soil parameters were estimated using the "sand" classification in Rosetta Lite. However, the saturated hydraulic conductivity (K_s) for soil materials was estimated through different means. The silt loam K_s value was estimated to be 9.6 cm hr^{-1} from infiltration tests done by Heeren et al. (2013). The K_s values for the gravel layers were determined using ERI data and the following relationship developed based on field data from the Barren Fork Creek site and one other floodplain site in the Ozark ecoregion (Miller et al. 2014; Miller, 2012):

$$K_s=0.11*\rho \quad (1)$$

where K_s is saturated hydraulic conductivity (m d^{-1}) and ρ is ERI resistivity (Ω-m). The K_s values for points within each gravel layer as determined with ERI data were then averaged to generate an average K_s for that layer. Average K_s values ranged between 130 cm hr^{-1} to 578 cm hr^{-1}.

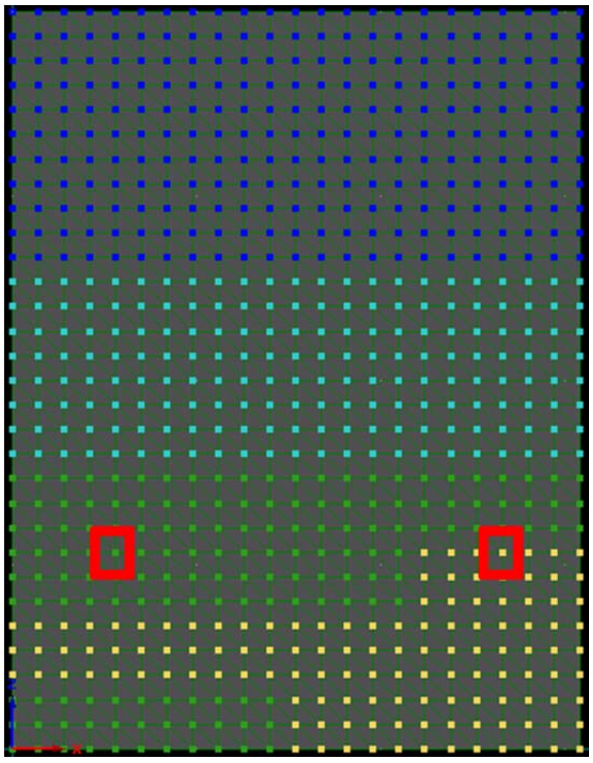

Figure 3. Material distribution represented in HYDRUS 3-D. Silt loam topsoil (dark blue) overlays three distinct gravel layers of different *Ks* from lowest (light blue) to highest (yellow). Observation nodes matching placement of observation wells from Heeren et al. (2013) are marked by red boxes.

In order to determine soil physical and chemical properties, soil core samples were collected with a Geoprobe Systems (Salina, KS) 6200 TMP (Trailer-mounted Probe) direct-push drilling machine using a dual-tube core sampler with a 4.45 cm opening. Before P injection experiments, background soil cores were collected during the installation of the observation wells from one to four wells per plot.

In the lab soil cores were sliced into approximately 15 cm samples representing different vertical horizons. All soils were air-dried and sieved with an 8 mm sieve prior to analysis. While a 2 mm sieve is commonly used, laboratory analysis showed that P sorption capacity was significant on the 2 to 4 mm and 4 to 8 mm particle size fractions as well as the less than 2 mm size fraction. The greater than 8 mm particle size fraction had only

a small capacity for P sorption and was difficult to analyze with regular soil chemistry lab procedures. Therefore, all soil chemistry testing was performed on the less than 8 mm fraction of each sample. Soil pH and electrical conductivity (EC) were determined with a 1:1 soil to de-ionized water solution, stirred with a glass rod and equilibrated for 30 minutes. All soil samples (approximately 670) were analyzed for water soluble (WS) P, Al, Fe, Ca, Mg, and Mn content (Figure 4). Water extractions were conducted by shaking air dried soil with de-ionized water (soil:solution ratio of 1:10) end over end for 1 h, followed by centrifuging (2500 rpm at 5 min) and filtration with 0.45 µm Millipore membrane. Extracted P, Al, Fe, Ca, Mg, and Mn were analyzed by inductively coupled plasma atomic emission spectroscopy (ICP-AES).

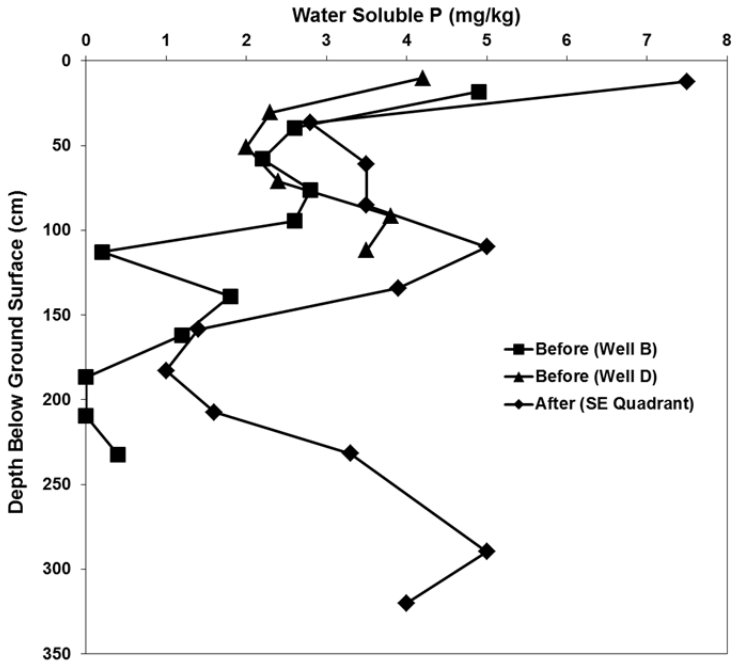

Figure 4. Subsurface soil water soluble P concentrations (mg P kg^{-1} soil) before and after plot experiments. Note the end of the P plume between 160 and 185 cm (Well B).

Oxalate extractable P, Al, Fe, and Mg (P_{ox}, Al_{ox}, Fe_{ox}, Mg_{ox}; 1:40 soil: 0.2M acid ammonium oxalate (pH 3), 2 h reaction time in the dark; McKeague and Day, 1966) were determined for all "topsoil" (approximately the top 10-15 cm of the soil core) samples. The P, Ca, Mg, K, Al, and Fe from ammonium oxalate extractions were measured using ICP-AES. Amorphous Al and Fe are considered to be the most reactive soil fraction in regard to P sorption. The ratio of ammonium oxalate extractable P to (Al + Fe) (all values in mmol kg^{-1}) was expressed as:

$$DPS_{ox} = \left[\frac{P_{ox}}{Al_{ox}+Fe_{ox}}\right] 100\% \quad (2)$$

where DPS_{ox} is the ammonium oxalate degree of P saturation (Table 1). Note that this is exactly the same as the traditional soil degree of phosphorus saturation (DPS) calculations (Pautler and Sims, 2000) except without the empirical constant α which is used to relate soil P sorption capacity to Al_{ox} and Fe_{ox} and the denominator acts to express the effective total soil P sorption maximum. The α value was unknown, so no α value was used. Beauchemin and Simard (1999) noted that various studies have applied an α value of 0.5 to all soils, regardless of soil properties. The authors claimed that the α value is empirical and needs to be determined for each soil type and experimental conditions. In addition, Beck et al. (2004) recommended that the α value be omitted from the DPS calculation.

Table 1. Soil chemical properties for the topsoil (approximately the top 10-15 cm of the soil core) at each plot location for both before and after the water and solute infiltration experiments. Data include electrical conductivity (EC) and the Degree of P Saturation (DPS), which was calculated based on the molar concentrations of the ammonium oxalate extract.

Plot	P Injection	n	pH	EC ($\mu S\ cm^{-1}$)	Water Soluble ($mg\ kg^{-1}$)				Ammonium Oxalate ($mg\ kg^{-1}$)				DPS (%)
					P	Al	Fe	Mg	P	Al	Fe	Mg	
1x1α	Before	2	6.3	97	4.6	192	40	9	223	621	2,050	101	12.0
	After	1	6.3	325	7.5	71	39	18	300	604	2,296	160	15.3
3x3α	Before	2	6.5	139	5.2	321	66	12	246	704	2,535	102	11.1
	After	3	6.5	134	4.9	198	52	10	269	643	2,373	129	13.1

Phosphorus adsorption isotherms were performed on background vadose zone samples from both the silt loam and the gravel subsoil. The P adsorption isotherms were conducted by adding different levels of P (0.0, 0.5, 1.0, 10, and 20 mg P L^{-1}) to 2 gram soil samples, equilibrating for 24 hr (shaking), and measuring P in the equilibrated, centrifuged, and filtered samples by ICP-AES.

While P isotherms are nonlinear and often characterized by the Langmuir equation, they typically exhibit linearity at low concentrations. Therefore, the low concentration data (less than 8 mg/L) were fit with a linear isotherm:

$$q=K_{d,<8mm}C_{eq}+y_{int,<8mm} \quad (3)$$

where q is the mass sorbed (mg P kg^{-1} soil), $K_{d,<8mm}$ is linear sorption coefficient for the fine fraction (L water mg^{-1} P), C_{eq} is the equilibrium solution P concentration (mg P L^{-1} water), and $y_{int,<8mm}$ is where the line intercepts the y-axis (L water kg^{-1} soil). Since the soil samples already had a significant amount of previously sorbed P, desorption occurred at low C_{eq} as indicated by negative values in a plot of q vs. C_{eq} (Figure 5). The y_{int} is an indication (though not equal to because of adsorption-desorption hysteresis) of the amount of P previously sorbed onto the soil sample at the time of sample collection. The equilibrium P concentration (EPC), where neither sorption nor desorption occurred, was calculated as the x-intercept of a logarithmic trendline fit to the entire data set (including high concentrations).

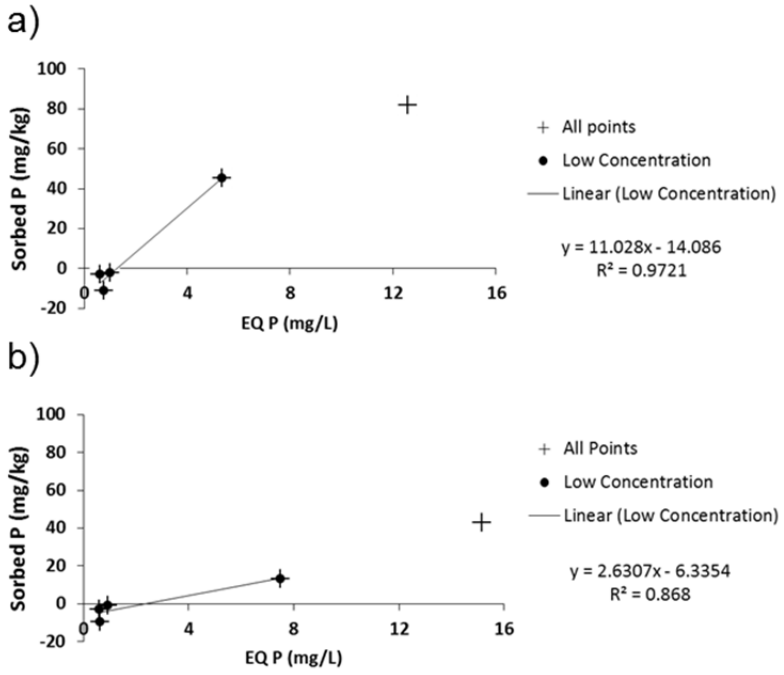

Figure 5. Phosphorus sorption isotherms for the Barren Fork Creek site for (a) silt loam, 64-83 cm below ground surface, and (b) sandy gravel, 142-163 cm below ground surface. See Table 2 for additional data for these samples.

Since the isotherms were performed on the less than 8 mm fraction, parameters were needed that

characterized the whole soil sample (Table 2) since HYDRUS calculates P sorption in terms of the entire soil mass. Sorption on the greater than 8 mm size fraction was assumed to be negligible. Therefore, "weighted" linear isotherm parameters were determined by accounting for the fraction of total sample on which testing was performed:

$$K_{d,whole}=f_{<8mm}(K_{d,<8mm}) \quad (4)$$

where $K_{d,whole}$ is linear sorption coefficient for the whole soil sample (L water mg^{-1} P), and $f_{<8mm}$ is the fraction of the soil sample that passes an 8 mm sieve (kg kg^{-1}). The $y_{int,whole}$ was weighted in the same way. The EPC is the same for the fine fraction and the entire sample.

Table 2. Soil physical and chemical properties for samples selected for phosphorus adsorption isotherms from the Barren Fork Creek site. Well B is part of the 1x1α plot, and Well K is part of the adjacent 3x3α plot (Heeren et al., 2013).

Borehole	Depth (cm)								
Soil Physical and P Sorption Characteristics									
						<8 mm fraction		weighted	
			8 mm sieve	EPC	K_d	y-int	K_d	y-int
		Soil type	(% passing)	(mg L^{-1})	(L kg^{-1})	(mg kg^{-1})	(L kg^{-1})	(mg kg^{-1})
Well B	64-83	Silt loam, some gravel	94	0.94	11.0	-14.1	10.3	-13.2
Well K	142-163	Sandy gravel	57	1.08	2.6	-6.3	1.5	-3.6
Soil Chemical Properties									
				Water Soluble					
		pH	EC	P	Al	Fe	Ca	Mg	Mn
			(µS cm^{-1})	(mg kg^{-1})	(mg kg^{-1})	(mg kg^{-1})	(mg kg^{-1})	(mg kg^{-1})	(mg kg^{-1})
Well B	64-83	6.3	26	2.8	799	113.1	74	18	2.7
Well K	142-163	6.4	10	2.7	321	89.4	17	10	1.7

Note than units in this HYDRUS simulation were cm for length, g for soil mass (i.e. bulk density in g cm^{-3}), and µg for P mass. Therefore, K_d was entered in units of cm^3/g (e.g. K_d = 10.3 L kg^{-1} = 10.3 cm^3 g^{-1} for the silt loam). The measured K_d for the gravel sample was applied to the whole gravel layer in HYDRUS. Initial conditions in HYDRUS included a soil solution P concentration equal to the EPC for the silt loam layer (0.94 mg L^{-1}) and the top of the gravel layer (1.08 mg L^{-1}). Initial solution P concentration in the gravel below the water table was equal to average of background P concentrations from well samples (0.055 mg L^{-1}). The disparity in these concentrations indicates the presence of a solute front in the soil matrix (from historical P leaching) that has not yet reached the water table, although P leaching through macropores may have reached the water table during rainfall events. Based on the relative location of this solute front which is apparent in the WSP data (Figure 4), a linear interpolation was used for the initial P concentration between 1.08 mg L^{-1} at 160 cm and 0.055 mg L^{-1} at 175 cm (Figure 7). Soil P was assumed to be in chemical equilibrium with the solution.

Calibration runtime parameters were modeled after field experiments done by Heeren (2012). Simulation data in HYDRUS was matched to data collected from selected observation wells at the Barren Fork 1x1α site (Figure 6). Observation nodes were placed at the water table on either side of the plot to represent the selected observation wells (Figure 3). Data from the wells were then used for calibration. Water and solute inflows were also set to match conditions in the Heeren (2012) study. Chloride (Cl) was used as an indicator for water flow in the Heeren (2012) study due to its nature as a conservative tracer and was simulated in HYDRUS alongside P. For Cl and P calibration, constant concentrations of 50.1 mg L^{-1} and 1.68 mg L^{-1} were used in each respective study. For both studies, a constant head of 6 cm was applied over the plot area.

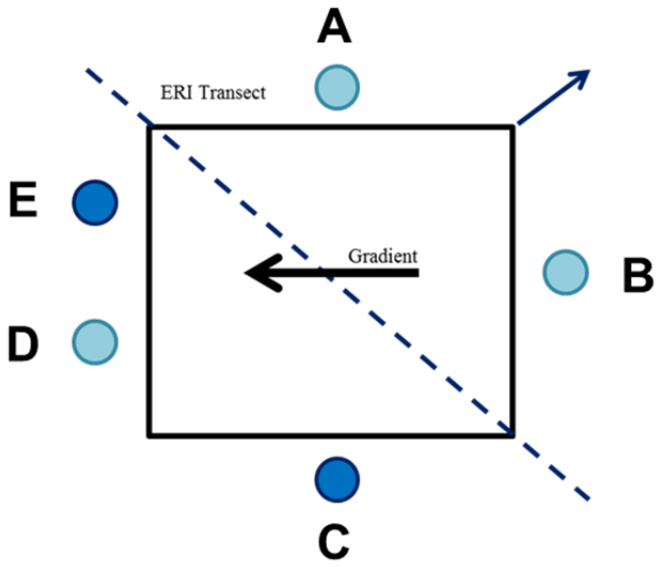

Figure 6. Plot overhead view. Path of ERI transect is indicated. Wells are labeled A-E. Observation wells selected for calibration indicated in dark blue.

Calibration of HYDRUS model

The θ_m and θ_{im} [L^3L^{-3}] terms represent the mobile and immobile phases of the soil pore space. They allow the model to divide the profile into two distinct phases: a mobile phase that is open to water flow and solute transport through advection and dispersion, and an immobile phase that prohibits water flow and solute transport within the immobile zone. Water exchange between the immobile and mobile zones is considered an apparent "diffusion" process, and solute exchange occurs by advection with the water exchange as well as molecular diffusion. In soil terms, the immobile phase is the soil matrix, while the mobile phase is made of fractures generated by weathering effects, root action, burrowing animals and insects, or bands of highly conductive materials that cut through the matrix. The θ_m and θ_{im} are complementary portions of the total porosity of the soil, such that:

$$n = \theta_{m,s} + \theta_{im,s} \quad (5a)$$

$$\theta = \theta_m + \theta_{im} \quad (5b)$$

where n is the total porosity [L^3L^{-3}], θ is the total unsaturated water content, $\theta_{m,s}$ and θ_m are the saturated and unsaturated mobile water content, and $\theta_{im,s}$ and θ_{im} are the saturated and unsaturated immobile water content. HYDRUS 3-D uses this distinction to modify the Richard's equation for multi-domain flow as follows (Šimůnek et al., 2003):

$$\frac{\partial \theta_{mo}(h_{mo})}{\partial t} = \frac{\partial}{\partial t}\left[K(h_{mo})\left(\frac{\partial h_{mo}}{\partial z} + 1\right)\right] - S_{mo}(h_{mo}) - \Gamma_w \quad (6a)$$

$$\frac{\partial \theta_{im}(h_{im})}{\partial t} = -S_{im}(h_{im}) + \Gamma_w \quad (6b)$$

where $\theta_{mo,\ im}$ are the water contents for the mobile and immobile phases [L^3L^{-3}], h_{mo} and h_{im} are the mobile and immobile pressure heads, respectively [L], $K(h_{mo})$ is the unsaturated hydraulic conductivity function for the mobile zone [$L\ T^{-1}$], t is time [T], z is the vertical coordinate, with positive in the upward direction [L], S_{mo} and S_{im} are mobile and immobile sink terms, respectively [-], and Γ_w is the water transfer rate between mobile and immobile phases [-].

Tension infiltrometer tests conducted by Heeren et al. (2013) showed that 99% of flow is directed through macropores at the Barren Fork site, and between 85% and 99% at similar sites in the Ozark ecoregion. Simulations conducted by Šimůnek et al. (2003) in HYDRUS suggested the possibility of such flows occurring through a mere 2.5% of total pore space, which suggested that macropores can have a dominant effect on subsurface flows. Reducing the flow domain to such a small space has dramatic effects on mean pore water velocity and would certainly cause water and solutes to arrive much sooner than through simple matrix flow, which is consistent with results found by Heeren (2012). Values of θ_m and θ_{im} were set to reflect the simulation conducted by Šimůnek et al. (2003) and flow effects were evaluated by increasing the mobile phase

contribution within the confines of the porosity suggested by the Rosetta Lite function (Table 3).

Table 3. Soil properties and calibration parameters.

	Soil Parameters					
		van Genuchten Parameters				
		Mobile			Immobile	
	K_s	α	n	l	α	n
	(cm hr^{-1})	(cm^{-1})	(-)	(-)	(cm^{-1})	(-)
Silt Loam	9.6	0.1	2	0.5	0.02	1.41
Gravel	130-578	0.145	2.68	0.5	0.145	2.68
	Calibration Parameters					
	$\theta_{m,s}$	Disp. L.	Disp. T.	ω	α	Frac
	(cm^3 cm^{-3})	(cm)	(cm)	(hr^{-1})	(hr^{-1})	(-)
Silt Loam	0.01-0.45	4-200	0.4-20	0.001-1	0.001-5	0-1
Gravel	0.01-0.43	4-200	0.4-20	0.001-10	0.001-5	0-1

Dispersivity [L] is used to correlate pore velocity to the mechanical dispersion of solutes in soil systems. Traditionally, longitudinal dispersivity has been approximated to be 10% of the sample length in the direction of flow, and transverse dispersivity being approximately 10% of the longitudinal dispersivity (Lallemand-Barres, 1978, as presented in Fetter, 1999). The flow path length during the field experiments was approximately 400 cm, resulting in a first estimate of longitudinal dispersivity of 40 cm. However, this approximation is based on fitting a trend line to observed data, which can vary from the trendline by half an order of magnitude or more (Lallemand-Barres, 1978, as presented in Fetter, 1999). Transverse dispersivity was not calibrated independently and was considered to be 10% of the longitudinal dispersivity value.

The ω [T^{-1}] and α [T^{-1}] terms are the water and solute mass transfer coefficients, respectively, for the mass transfer function in the modified advection-dispersion equation presented by Simunek et al.(2003):

$$\frac{\partial \theta_{mo} c_{mo}}{\partial t} + f_{mo}\rho \frac{\partial s_{mo}}{\partial t} = \frac{\partial}{\partial z}\left(\theta_{mo} D_{mo} \frac{\partial c_{mo}}{\partial z}\right) - \frac{\partial q_{mo} c_{mo}}{\partial z} - \varphi_{mo} - \Gamma_s \quad (7a)$$

$$\frac{\partial \theta_{im} c_{im}}{\partial t} + \left(1-f_{mo}\right)\rho \frac{\partial s_{im}}{\partial t} = \Gamma_s - \varphi_{im} \quad (7b)$$

where $c_{mo,\ im}$ are the concentrations of solute in the mobile and immobile phases [ML^{-3}], s_{mo} and s_{im} are the sorbed concentrations of solute in the mobile and immobile phases [ML^{-3}], f_{mo} is the fraction of sorption sites in contact with mobile water [-], D_{mo} is the dispersion coefficient for the mobile phase [L^2T^{-1}], $\varphi_{mo,\ im}$ are lump sink-source terms for the mobile and immobile phases, and Γ_s is the mass transfer function, defined as:

$$\Gamma_s = \alpha\left(1-w_{im}\right)\left(c_{mo}-c_{im}\right) + \Gamma_w c^* \quad (8a)$$

where α is the solute mass transfer coefficient [T^{-1}], w_{im} is the ratio of the volumes of the matrix and the total pore systems, $\theta_{ms}\,\theta_s^{-1}$[-], c^* is equal to c_{mo} for $\Gamma_w>0$ and c_{im} for $\Gamma_w<0$, and Γ_w is defined as:

$$\Gamma_w = \omega\left[S_e^m - S_e^{im}\right] = \alpha_w\left[h_m - h_{im}\right] \quad (8b)$$

where ω is the water mass transfer coefficient [T^{-1}], $S_e^{\ m}$ and $S_e^{\ im}$ are the effective saturation values for the mobile and immobile phases [-], h_m and h_{im} are the head pressures of the mobile and immobile phases [L], and α_w is a first-order mass transfer coefficient [T^{-1}].

Values of α are traditionally believed to be between 0.1 and 5.0 hr^{-1} as presented by Radcliffe and Šimůnek (2010); however, results from Alletto et al. (2006) found α to range between 0.0006 and 0.0424 h^{-1}, and Cheviron and Coquet (2008) reported α values of 0.0192 to 0.6528 hr^{-1}. Given these results, breakthrough curves (BTCs) were analyzed with α ranging over several orders of magnitude (Table 3). The ω term is not as well understood as α within the confines of modeling. One study by González-Delgado and Shukla (2014) could not find any trend matching ω to increasing pore water velocity with Cl tracers, and reported ω values of 0.001 to 0.30 hr^{-1} in loam and 0.20 to 1.02 hr^{-1} in sand. Therefore, BTCs were analyzed with ω ranging over several orders of magnitude with a minimum of 0.001 for both silt loam and gravel (Table 3).

Frac [-] is the fraction of sites available for sorption that are governed by an equilibrium process. The *Frac*

variable in HYDRUS-2D/3D has two functions, denoting either the fraction of sites available for instantaneous sorption during chemical non-equilibrium or the fraction of sites in contact with mobile water during physical non-equilibrium. Given the mobile-immobile nature of this particular model, *Frac* was used to denote the latter. *Frac* was analyzed over the entire range of possible values to get a good understanding of its effect on P sorption (Table 3). Due to the conservative nature of the Cl tracer, this variable was not calibrated when simulating Cl transport.

In addition to calibrating the dual-porosity model with distinct gravel layers, three additional models were considered. Calibration was performed using the default single-porosity model (van Genuchten-Mualem) in HYDRUS-2D/3D, both with a homogeneous gravel layer and heterogeneous gravel layers, as well as a dual-porosity model with a homogenous gravel layer. This was done to evaluate the effects of incorporating macropore flow (dual-porosity) and increasing model resolution (homogeneous gravel vs. heterogeneous gravel layers) on breakthrough time and overall shape of Cl and P BTCs. Soil properties for the homogeneous gravel layer were determined as area-weighted averages of the three distinct gravel layers found using ERI data.

Long-term P Modeling:

Long-term P transport was simulated in HYDRUS following the calibration process. A 100-cm wide, 300-cm deep 2D column was developed for the long-term model, corresponding to the vadose zone of the soil profile directly under the 100-cm wide plot used in calibration. Long-term P transport to the water table, situated at the bottom of the profile, was of interest. Boundary conditions were set so that the sides of the column were no-flow boundaries, the bottom of the column was a constant head boundary set to maintain a constant long-term water table elevation, and the top of the column was set as a variable flux boundary to simulate rainfall events. Initial conditions set the soil water in the column at hydrostatic equilibrium with the water table, and initial concentrations remained the same as those used for P calibration (Figure 7).

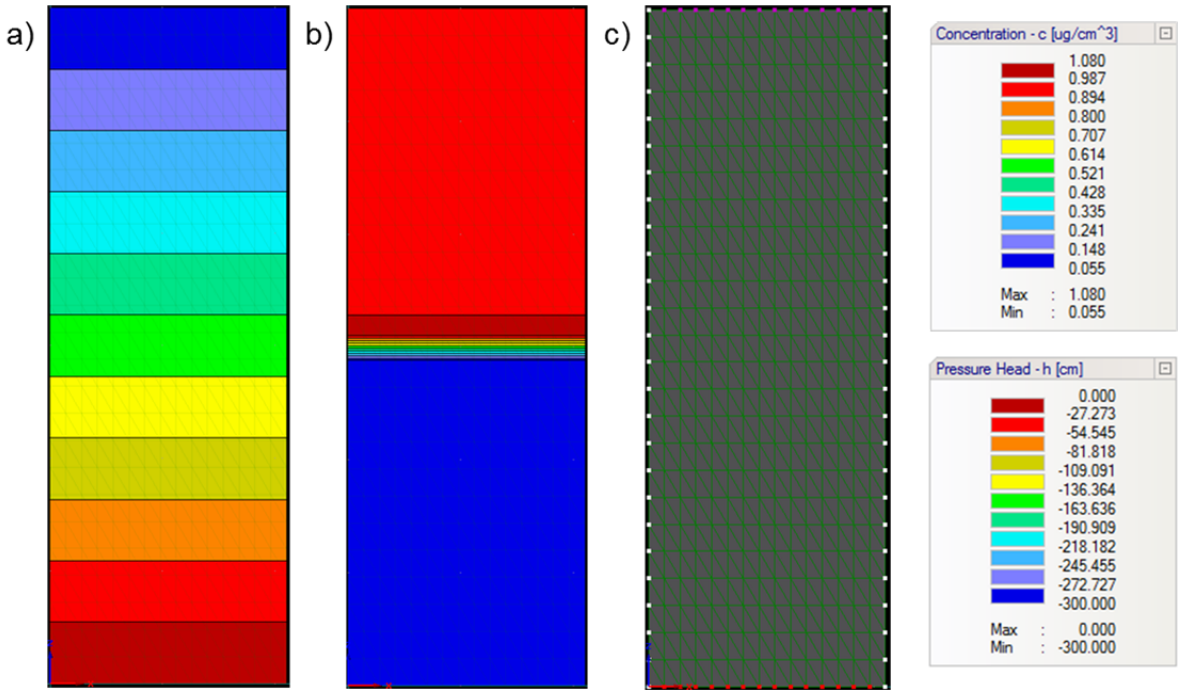

Figure 7. Initial and boundary conditions for long-term P modeling. Initial conditions for (a) pressure head and (b) mobile P concentration are shown, as well as (c) boundary conditions for variable flux (magenta) and constant head (red).

Rainfall was applied as daily totals estimated as constant rainfall intensities (cm hr^{-1}) over the entire 24 hour period. Nine years of daily rainfall data (Mar 2004-Mar 2013) were obtained from the Oklahoma Mesonet. Evapotranspiration was not simulated.

Phosphorus from poultry litter application was simulated as P applied with infiltrating rainwater. P was applied with infiltrating rainwater starting March 1st of each year to match traditional fertilizer application times. Each year, 61.9 mg of P were added to the column. This yearly application of P is consistent with a 2 ton per acre application rate of poultry litter on grass and a P content of 12.7 kg P per ton of litter as recommended by the Oklahoma Cooperative Extension Service (2013) and near the range of 13-27 kg P per ton of litter reported by MidWest Plan Service (2001). Initial concentrations of P in the simulated infiltration started at 15 mg L^{-1}, which

is consistent with P concentrations in the first post-litter application runoff event found by DeLaune et al. (2004). A linear relationship was developed between concentration and cumulative rainfall to simulate a decreasing water concentration from the poultry litter throughout the year at the soil surface:

$$C=-0.182R+15 \quad (9)$$

where C is the concentration (μg cm^{-3}) at the given time step, and R is the cumulative rainfall (cm) since March 1st of the year. Once the applied P reaches 61.9 mg, no more additional P was added to rainwater for that year. In the event that rainfall was insufficient to remove all P from the surface for a given year, the excess P was added to the next year and a new linear relationship was developed to reflect the extra P.

Long-term modeling was also done using high-resolution rainfall data. Rainfall totals recorded on a five minute basis were obtained from the Oklahoma Mesonet for the Mar 2004-Mar 2013 period. Given the large volume of rainfall data points, simulations were limited to one year at a time, with initial and boundary conditions imported from the previous year to effectively simulate nine continuous years of rainfall.

Results

Calibration Results

Calibration was performed for both Cl and P transport. Calibration results were compared to breakthrough time and the overall trend of the observed data, and the best fit overall between the two calibration criteria was used to set the baseline parameter values for sensitivity analysis and long-term testing (Figure 8). Best-fit parameter values can be found in Table 4. Simulations adequately matched observed data from the Barren Fork 1x1α site. The effects of minimizing and maximizing ω and α on the shape and timing of the breakthrough curve were also analyzed (Figure 9). One limitation of the model was the inability to match observed data with reasonable *Frac* values. Predicted values of *Frac* were about 0.03, which is consistent with the percent macropore composition of the soil profile. However, simulated values of *Frac* had to be set close to 1 to achieve reasonable breakthrough times for P and remain consistent with Cl calibration results.

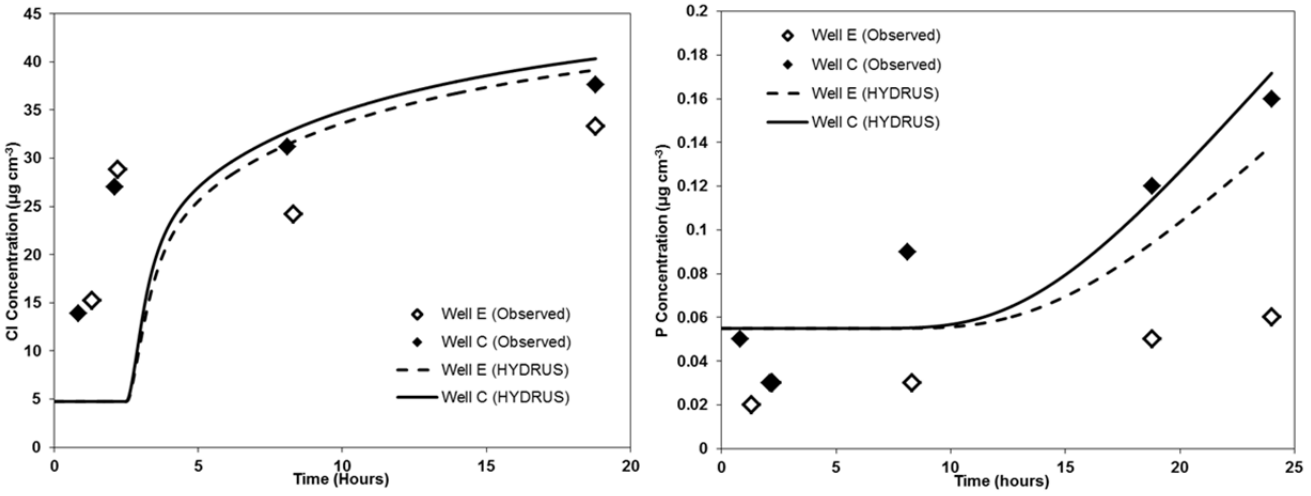

Figure 8. Calibration results for Cl (left) and P (right). Curves are HYDRUS-generated BTCs, points are observed data from Heeren et al. (2012).

Calibration results were limited in matching the model to observed data. Breakthrough times were difficult to match for the Cl and P simultaneously. While breakthrough times for Cl were relatively short, breakthrough times for P were relatively long. Balancing parameters that managed water flow, such as ω, was a difficult task as changing these parameters to better match one solute caused a poor match with the other. Solute transport parameters, such as soil isotherm properties, were not enough to balance the Cl and P perfectly.

In addition to this, HYDRUS was unable to fully simulate the differentiation between observation wells C and E. Observation data showed that both wells received some level of Cl, but only well C recorded any significant P increase. While the P increase simulated by HYDRUS in well E was reduced by comparison to well C, the increase simulated was still far above the trend defined by observed data (Figure 8).

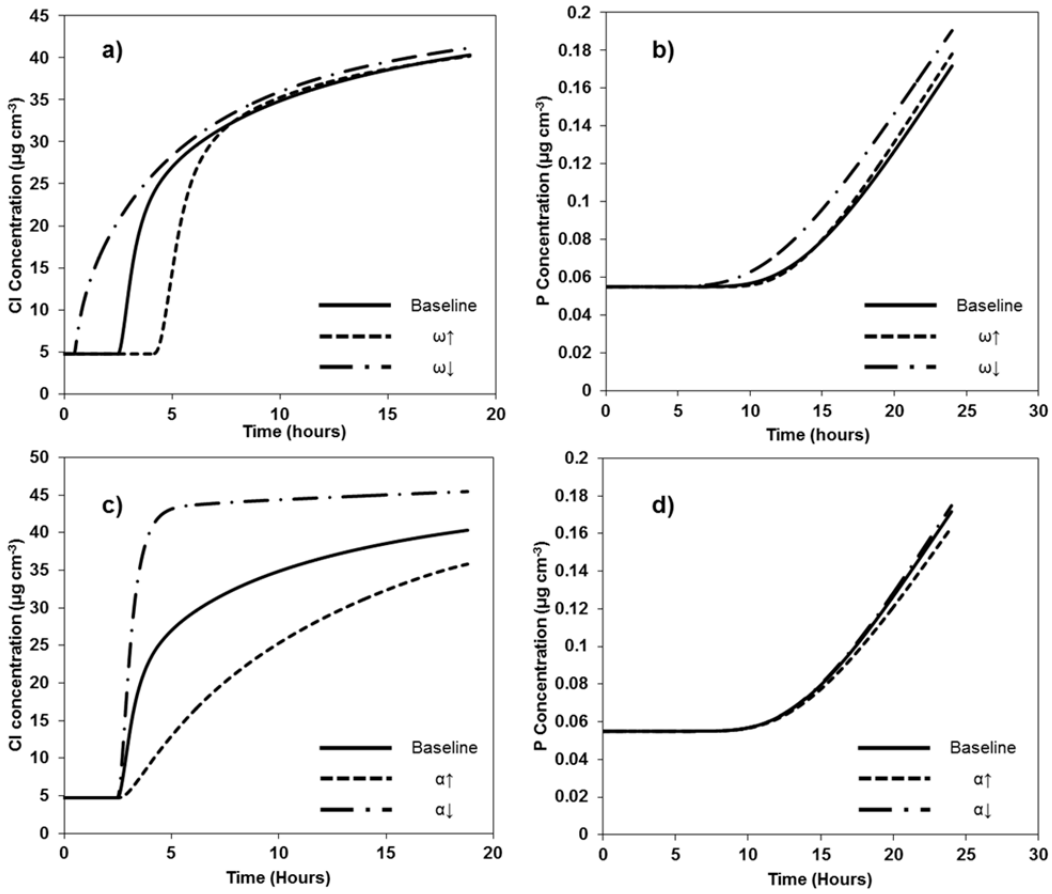

Figure 9. Analysis of *ω* effects on (a) Cl and (b) P, and *α* effects on (c) Cl and (d) P. Note that decreasing *ω* increases breakthrough time for both Cl and P, and increasing *ω* has the opposite effect. Effects of *α* are more complex; decreasing *α* makes Cl breakthrough sharper, but has little effect on breakthrough time, but increasing *α* effects both time and shape of Cl breakthrough. No effect is seen in P breakthrough. Analysis was performed on Well C data.

Mass balance information for the calibration was also collected. Peclet and Courant numbers were analyzed for potential model instability. Peclet numbers for the Cl and P were between 0.22 and 0.23, which is lower than the maximum Peclet number of 5 recommended by Radcliffe and Šimůnek (2010). Courant numbers for the Cl and P were below 0.003, which is less than the maximum Courant number of 1 recommended by Radcliffe and Šimůnek (2010). Water mass balance error for the Cl and P calibrations were near 24%, and adjustments to mesh size, time steps, or iteration criteria were unable to reduce this imbalance. Water mass balance remains a potential limitation of this particular model. Solute mass balance errors were far more favorable, with a Cl mass balance error of 1.4% and a P mass balance error of 0.02%.

Table 4. Final parameter values from calibration results.

	Calibration Parameter Results					
	$\theta_{m,s}$	Disp. L.	Disp. T.	ω	α	Frac
	($cm^3\ cm^{-3}$)	(cm)	(cm)	(hr^{-1})	(hr^{-1})	(-)
Silt Loam	0.01	100	10	0.01	0.2	1
Gravel	0.01	200	20	0.1	0.01	1

Calibration results for three additional models were also analyzed within HYDRUS (Figure 10) and compared to the “standard” dual-porosity model with heterogeneous gravel layers. The single porosity (van Genuchten-Mualem) model with a homogeneous gravel layer produced BTCs with longer breakthrough times, reduced peak concentrations, and poor differentiation between the two observation wells (Figures 10a and 10b). The single porosity model with heterogeneous gravel layers performed slightly better; while still having poor breakthrough times and peak concentrations, this model showed better differentiation between the two

observation wells (Figures 10c and 10d). Calibration parameters for these two models were limited to the longitudinal and transverse dispersivity for the silt loam; all other variables either belong to the dual-porosity model or were already set to their maximum value prior to calibration. Silt loam Disp. L. and Disp. T. were set to maximum value established in Table 3 to produce these results.

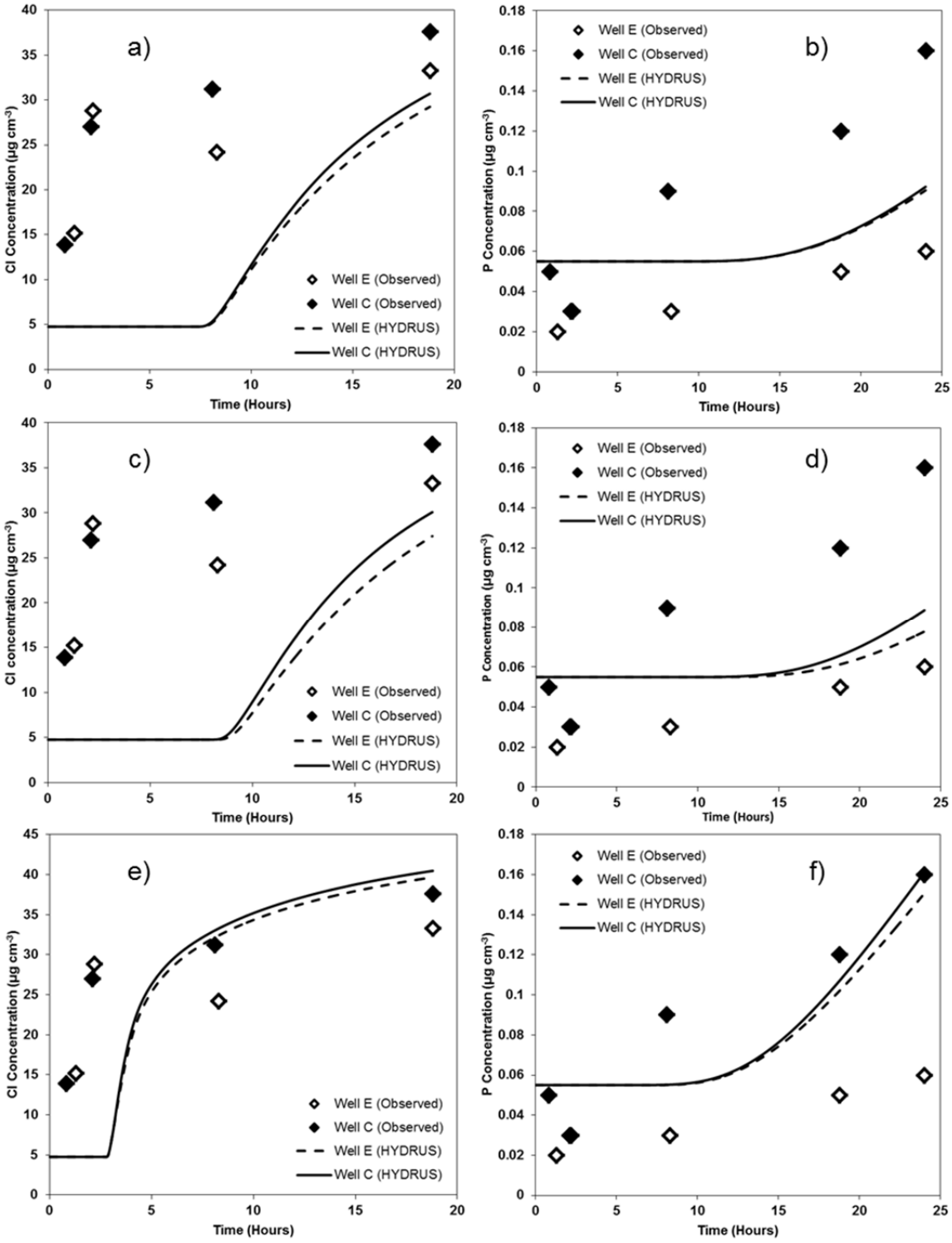

Figure 10. Calibration of Cl (a, c, e) and P (b, d, f) for three additional models in HYDRUS-2D/3D. Simulations included a single porosity (van Genuchten-Mualem) model with a single average gravel layer (a, b); a single porosity (van Genuchten-Mualem) model with three distinct gravel layers defined by ERI data (c, d); and a dual-porosity model with a single averaged gravel layer (e, f). The dual porosity with three distinct gravel layers defined by ERI data is shown in Figure 8 and was selected for the long term simulations.

The last model evaluated was the dual-porosity model with a homogeneous gravel layer (Figures 10e and 10f). Most of the parameters remained consistent with the "standard" dual-porosity model used for the long-term simulations, however the mobile sorption site fraction was re-calibrated for this model. Breakthrough times and peak concentrations for Cl were similar to the "standard" dual-porosity model, although breakthrough time lagged behind by about 30 minutes and differentiation between the wells was poorer. The P calibration was much closer to the "standard" model, with the added benefit of having a lower Frac value of near 0.75. Despite this, there is still poor differentiation between observation wells and the Frac value is still not low enough to consider using this model over the "standard" model.

Sensitivity Analysis

A sensitivity analysis was performed standard model to determine the impact of each parameter on breakthrough time for both Cl and P transport. Each solute simulation was analyzed with respect to the time taken for water at the well C observation node to reach a concentration of 15 mg L^{-1} for Cl (t_{15}) or 0.12 mg L^{-1} for P ($t_{0.12}$). Parameters were then increased or decreased and the percent change in t_{15} or $t_{0.12}$ was recorded. Results were plotted as percent change in the parameter from the baseline value against percent change in time to the target concentration (Figures 11 and 12).

For Cl modeling, longitudinal dispersivity and immobile pore fraction had an inverse relationship to t_{15}, while α and ω had a positive relationship to t_{15}, although both α and ω seemed to display asymptotic behaviors at large percent increases in the variable. The most sensitive parameters for the Cl analysis were $\theta_{s,im}$ for both the silt loam and the gravel, with a maximum increase in t_{15} of 77% and 167%, respectively. The least sensitive parameter was α for the silt loam, which despite seeing a 400% increase in value only produced a 4% increase in t_{15} (Figure 11).

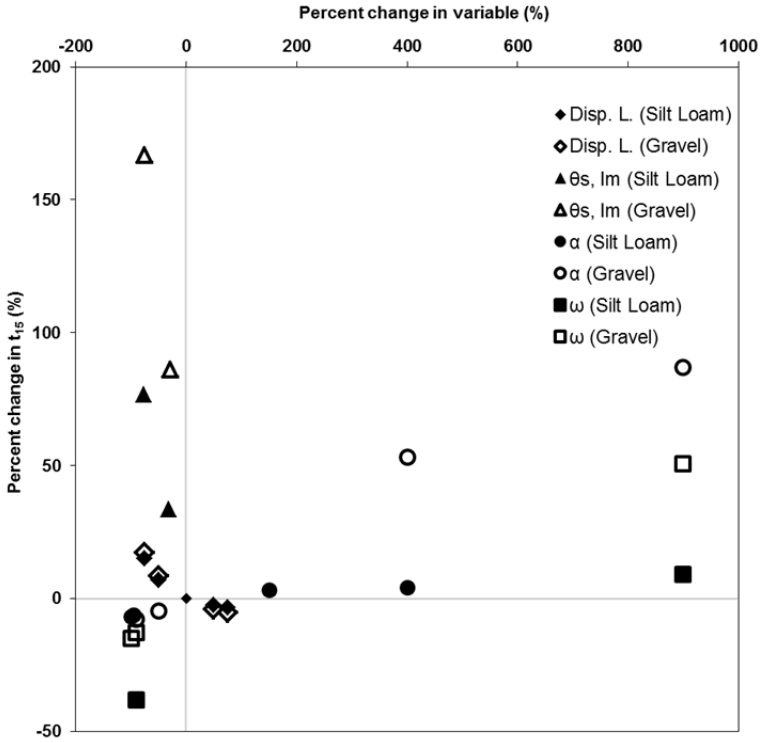

Figure 11. Sensitivity analysis for Cl simulations.

For P modeling, gravel mobile sorption site fraction and gravel adsorption isotherm coefficient had a positive relationship to $t_{0.12}$. Neither mobile site sorption fraction or adsorption isotherm coefficient for the silt loam layer had any significant effect on $t_{0.12}$. Although soil chemical analysis showed that the soils were not close to P saturation (DPS < 16%, Table 1), initial solution P concentration in the silt loam (0.94 mg L^{-1}) was high relative to the plot inflow P concentration (1.68 mg L^{-1}). This initial condition would significantly reduce the impact of silt loam-dependent parameters, as sorption sites are already mostly filled with P for the inflow concentration. The gravel mobile sorption site fraction was the most sensitive parameter, with a maximum of 70% decrease in $t_{0.12}$.

The least sensitive parameters were gravel adsorption isotherm coefficients, with changes between -20% and 20% in $t_{0.12}$ over a wide percent change in the variable (Figure 12).

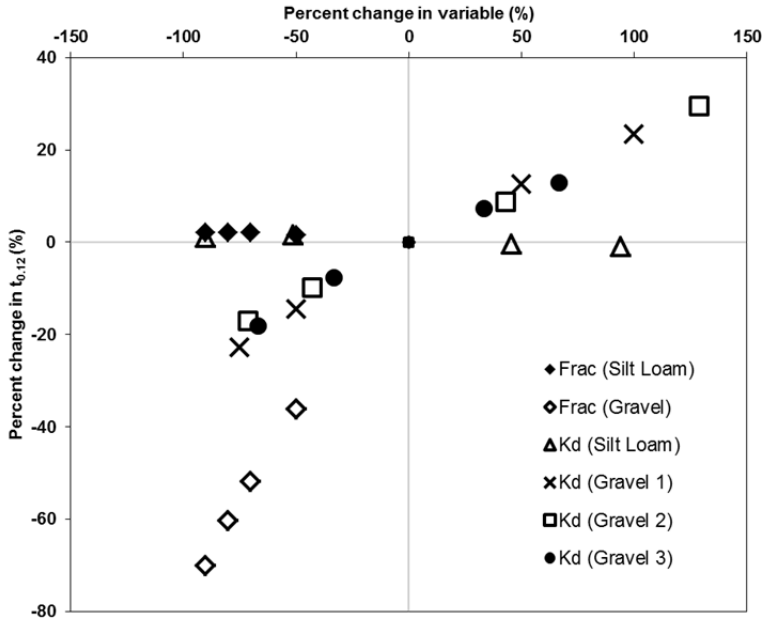

Figure 12. Sensitivity analysis for P simulations.

Long-term P modeling

Long-term modeling using daily precipitation data was conducted to determine the P loading to the water table between March of 2004 and March of 2013. Over nine years, approximately 546.5 kg ha^{-1} P was applied to the plot area through simulated fertilizer application. P mass was recorded as it crossed the water table boundary. Approximately 92 kg ha^{-1} P was lost to the water table, or about 17% of applied P (Figure 13).

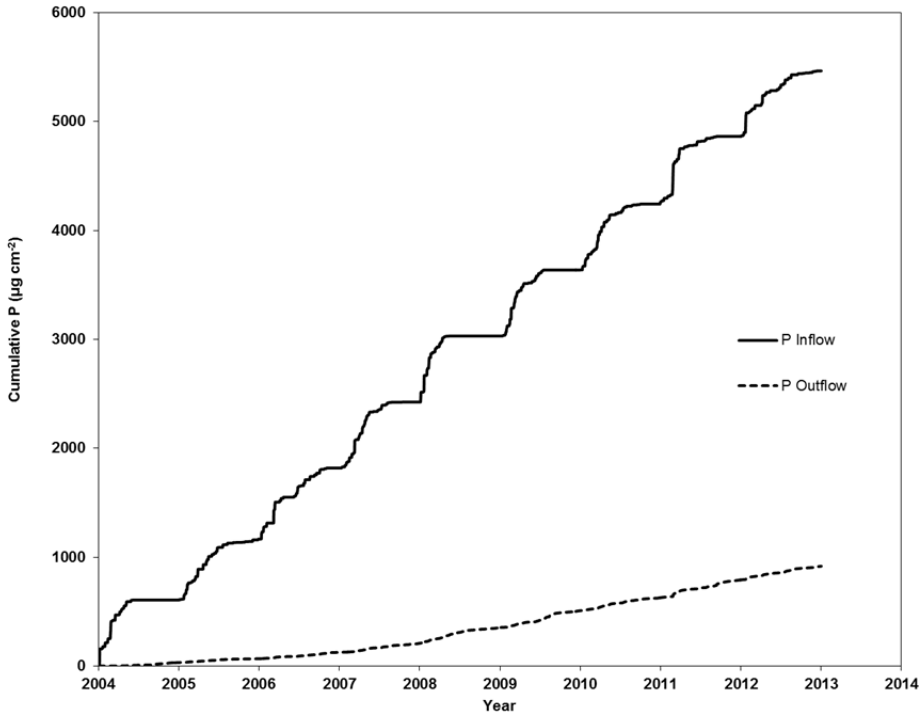

Figure 13. Cumulative P inflow from infiltration and cumulative P outflow into the water table for the dual-porosity daily rainfall model.

P concentrations of flow into the water table were analyzed in addition to P mass totals (Figure 13). P concentration of the flow into the water table steadily increased with time, with an end concentration of 1.74 mg L^{-1}. Wet years (2004, 2008, and 2009) saw significantly higher increases in concentration than average and dry years (Figure 14a). Sharp peaks indicate instances where P transport to the water table was higher than normal. Peaks tended to occur 15-40 hours after a large rain event and always preceded a larger volume of solute moving into the water table. This behavior could be indicative of a "first-flush" effect facilitated by the soil macropore network, allowing a large quantity of solute to move through the profile quickly. P concentration was also evaluated between 2008 and 2009 to determine which parts of the year are responsible for the highest increase in P. Phosphorus concentrations climbed steadily between the months of April and July in conjunction with the wet period of the year and summer storm events. Winter events between January and March also seemed to contribute significantly to P increases. Concentration increases declined after July, although several peaks can be seen that result from large scattered rain events (Figure 14b).

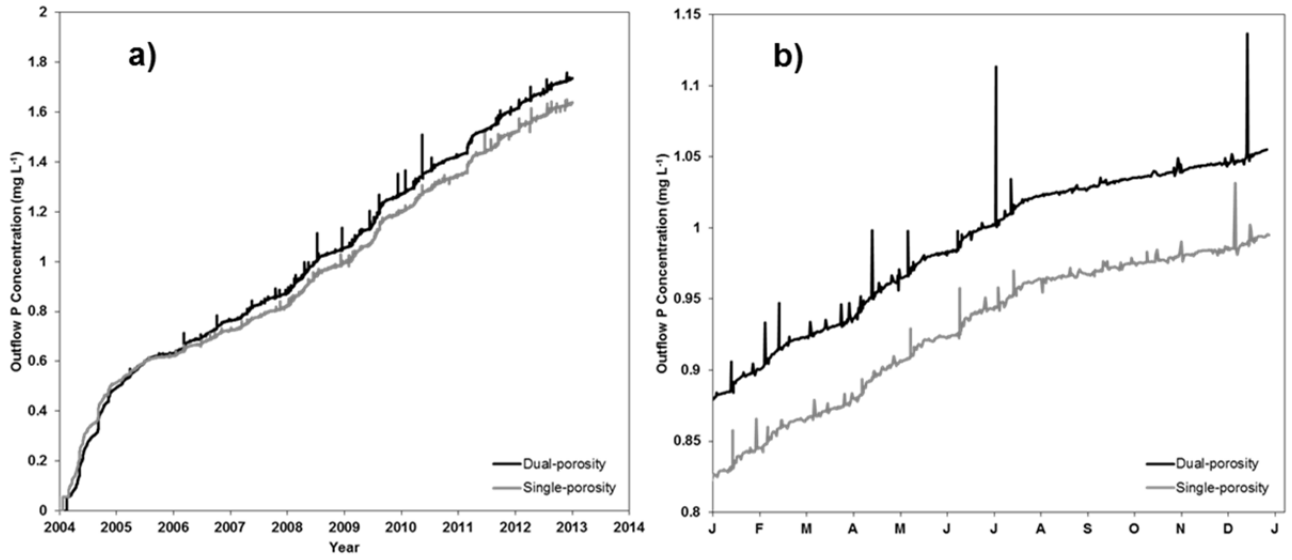

Figure 14. Simulated P concentration increases over time with the dual-porosity daily rainfall model between 2004 and 2013 (a) and for 2008 (b). Results for the single-porosity simulation are in gray.

Mass balance information was also collected for the long-term simulations. Peclet and Courant numbers of 0.093 and 0.03, respectively, were reported and are well within the stability ranges recommended by Radcliffe and Šimůnek (2010). Water mass balance error was acceptable at 0.71%, while P mass balance error was higher at 4.1%, but still acceptable for a complex subsurface system.

Long-term modeling was also done with the single-porosity model. Over 9 years, approximately 87,000 µg of P was lost to the water table, or 16% of applied P. However, the single-porosity model modeled a lower final P concentration at the water table of 1.64 mg L^{-1}, which is 0.1 mg L^{-1} less than the dual-porosity model predicted. The single porosity model also had fewer spikes in concentration and the peaks associated with these spikes were often less intense than those seen in the dual-porosity model (Figure 14a and 14b). Combined with the results of the calibration tests, this suggests that the dual-porosity model is working as intended, but some other factor was preventing the macropores from activating and transporting P properly to the water table.

Results from long-term simulations using 5-minute rainfall data showed greater P delivery to the water table than the other models. Over a period of nine years, 113 of the 544.4 kg ha^{-1} of P applied entered the water table (Figure 15). This corresponded to a 21% delivery rate of P, which was 23.5% higher than the dual-porosity model with daily rainfall totals.

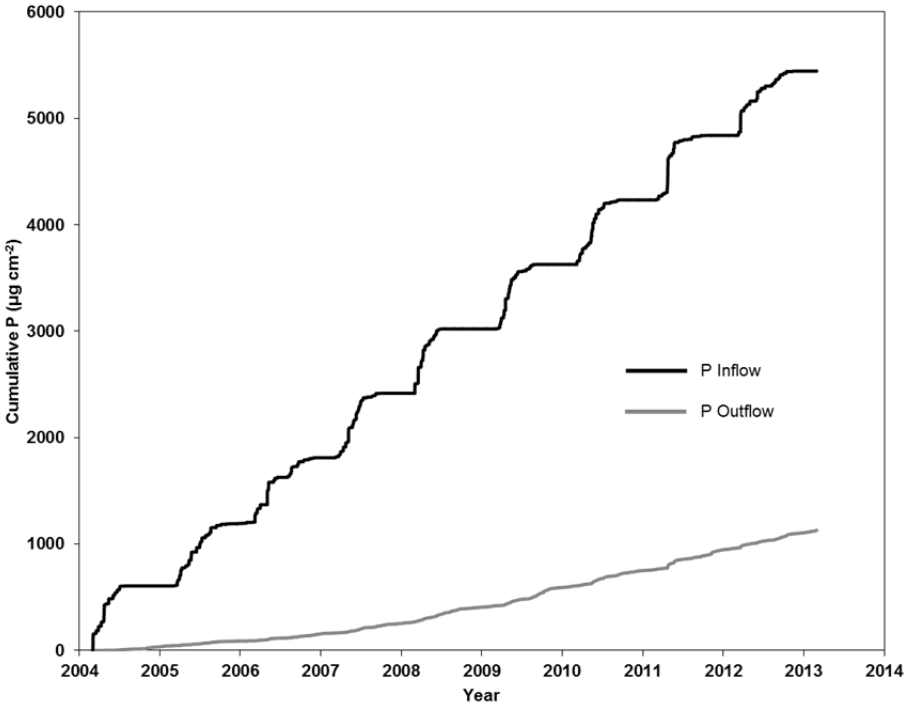

Figure 15. Cumulative P inflow from infiltration and cumulative P outflow into the water table for the dual-porosity 5-minute rainfall model.

P concentrations at the water table were recorded over the nine year period for the 5-minute rainfall model. The final P concentration was slightly higher than the daily rainfall model at 1.82 mg L^{-1}. The 5-minute rainfall model also reported higher P concentrations at the water table throughout the entire nine year period (Figure 16a). The 5-minute rainfall model simulated rapid delivery of P and water through macropores more effectively than the daily rainfall model. The concentration spikes associated with high-intensity storm flow through macropores were more numerous than the daily rainfall model, and the peaks of these spikes were much higher, suggesting better modeling of macropore flow with the 5-minute rainfall data. An analysis of concentration increase over 2008 shows these concentration spikes in more detail and compares them to a similar trend for the daily rainfall model (Figure 16b).

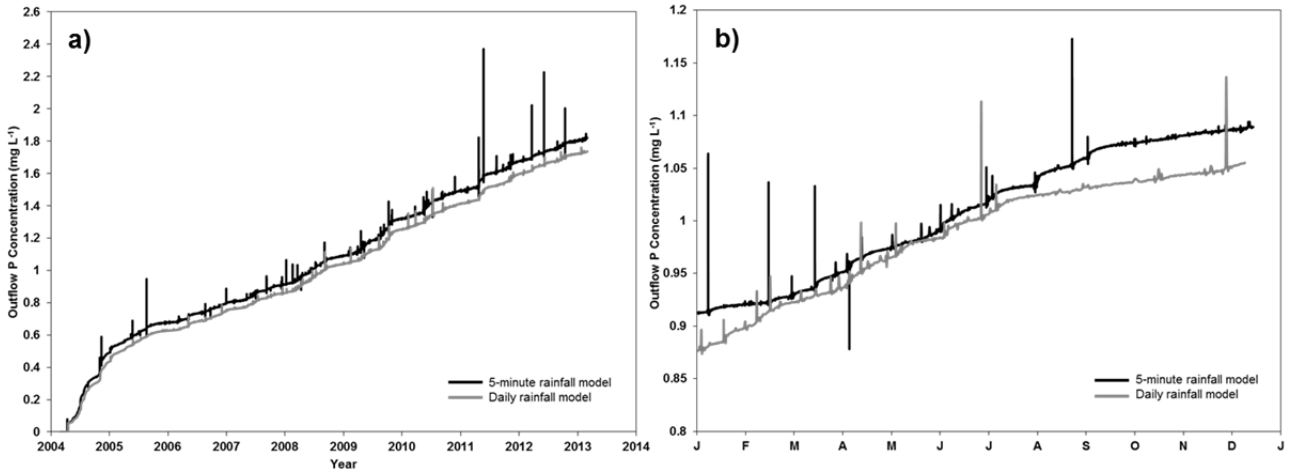

Figure 16. Simulated P concentration increases over time with the dual-porosity 5-minute rainfall model between 2004 and 2013 (a) and for 2008 (b). Results for the dual-porosity daily rainfall model are in gray.

Discussion

Calibration

HYDRUS had some difficulty matching simulation curves to observed data. It may be due to a lack of soil profile data collected by ERI. It is possible that the ERI survey missed some heterogeneity in the profile near the position of well C, which would have allowed P to reach the well faster than other points in the profile. It is also possible that the ERI data could not provide a fine enough resolution of the soil profile to catch heterogeneity that would have explained why only one well displayed P transport. Another explanation might be that the dual-porosity model simply is not sophisticated enough to model this system, and that alternative modeling techniques might need to be developed to handle profiles dominated by preferential flow.

Despite these limitations, HYDRUS was successful in modeling Cl and P transport. Chloride and P transport were modeled satisfactorily while still keeping the values of soil properties within accepted ranges. The success of this complex model in matching observed data confirms the usefulness of this model and certainly holds it above other subsurface models that cannot account for 2D or 3D flow.

The calibration of the three additional models and their comparison to the “standard” model suggest the usefulness of sampling techniques such as ERI surveying, and the necessity of using some dual-porosity model to accurately represent macropore flow. Results from the calibration suggest that modeling highly porous and variable soil systems such as these requires the highest resolution data available. In fact, while the ERI survey provided a higher resolution of data than can be found with many other data collection methods, even higher levels of resolution may be needed to more accurately model these complex systems. Calibration with models not featuring a dual-porosity system fell far short of observed data, underlining the need for some kind of multi-domain component to any model used to simulate soils with even a moderate level of macropore activity.

Long-term Simulation

The long-term simulations were successful in demonstrating macropore flow with the dual-porosity model. While the single-porosity model delivered nearly as much solute as the dual-porosity model did, the way in which the dual-porosity model delivered the P shows the usefulness of the dual-porosity model to simulate macropore flow.

The effectiveness of the dual-porosity model in modeling macropore flow increased when the daily rainfall data was replaced with 5-minute interval rainfall data. The use of this rainfall data generated more accurate storm events with higher intensities of rainfall than were seen when using the daily rainfall data. With higher intensity rainfall, the model was able to more accurately simulate the activation of macropore regions and had more success in simulating P transport to the water table. It is hypothesized that the low rainfall intensities resulting from 24-hr data allowed too much time for water and solute to diffuse from macropores into the soil matrix. The 5 minute rainfall data allowed for a more accurate simulate of rapid transport of water and solutes through macropores to the water table. The importance of using high-resolution rainfall data was demonstrated with the results of this simulation.

Future Work

Simulations with higher resolution rainfall data are needed to increase the accuracy of the model and better simulate macropore flow. However, the minimum level of resolution needed to accurately simulate macropore flow is unknown. Future work with regards to this model would focus on identifying that minimum level of resolution to produce significant results with the dual-porosity model. Another facet of this research will look to simulate macropore flow in ways other than the use of a dual-porosity model. Incorporating a “mesh-macropore” into the profile, simulated as a thin highly conductive pipe in HYDRUS, might offer more accurate results for highly porous systems and for soils that experience significant earthworm activity.

Acknowledgements

The authors gratefully acknowledge the support of the U.S. Geological Survey with a 104(g) grant and the University of Nebraska - Lincoln for a graduate research assistantship. The authors would also like to acknowledge Dr. Guillermo Baigorria for his help and advice with this research.

References

Alletto, L., Coquet, Y., Vachier, P. & Labat, C. (2006). Hydraulic conductivity, immobile water content, and exchange coefficient in three soil profiles. *Soil. Sci. Soc. America J.* 70(4): 1272-1280.

Beauchemin, S. & Simard, R. R. (1999). Soil phosphorus saturation degree: review of some indices and their suitability for P management in Quebec, Canada. *Canadian J. of Soil Sci.* 79: 615-625.

Beck, M. A., Zelazny, L. W., Daniels, W. L., & Mullins, G. L. (2004). Using the Mehlich-1 extract to estimate soil phosphorus saturation for environmental risk assessment. *Soil Sci. Soc. of America Journal* 68: 1762-1771.

Beven, K. & Germann, P. (1982). Macropores and water flow in soils. *Water Resources Res.* 18(5): 1311-1325.

Cheviron, B. & Coquet, Y. (2008). Sensitivity analysis of HYDRUS-1D to transient-MIM parameters: a case study related to pesticide fate in soil. *Second HYDRUS Workshop.* Prague, Czech Republic.

Cooper, A.B., Smith, C. M., & Smith, M. J. (1995). Effects of riparian set-aside on soil characteristics in an agricultural landscape: Implications for nutrient transport and retention. *Agr. Ecosyst. Environ.* 55(1): 61-67.

Correll, D. A., Heeren, D. M., Fox, G. A., Storm, D. E., Penn, C. J., & Halihan, T. April 4-5, 2013. Transient resistivity imaging of a phosphorous tracer test. *Geological Society of America South-Central Regional Meeting*, Austin, Tex.

DeLaune, P. B., Moore, Jr., P. A., Carman, D. K., Sharpley, A. N., Haggard, B. E., & Daniel, T. C. (2004). Development of a phosphorus index for pastures fertilized with poultry litter: Factors affecting phosphorus runoff. *J. Environ. Qual.* 33(6): 2183-2191.

Djodjic, F., Borling, K., & Bergstrom, L. (2004). Phosphorus leaching in relation to soil type and soil phosphorus content. *J. Environ. Qual.* 33: 678-684.

Fetter, C. W. (1999). *Contaminant Hydrogeology, 2nd Ed.* Long Grove, Ill.: Waveland.

Fox, G. A., Heeren, D. M., Miller, R. B., Mittelstet, A. R. & Storm, D. E. (2011). Flow and transport experiments for a streambank seep originating from a preferential flow pathway. *J. Hydrol.* 403: 360-366, DOI: 10.1016/j.jhydrol.2011.04.014.

Fuchs, J. W., Fox, G. A., Storm, D.E., Penn, C. J., & Brown, G. O. (2009). Subsurface transport of phosphorus in riparian floodplains: Influence of preferential flow paths. *J. Environ. Qual.* 38: 473-484. DOI: 10.2134/jeq2008.0201.

Gburek, W.J., Barberis, E., Haygarth, P. M., Kronvang, B., & Stamm, C. (2005). Chapter 29: Phosphorus mobility in the landscape. In Phosphorus: Agriculture and the Environment, 941-979. Sims, J.T. and A. N. Sharpley, ed. Madison, Wis.: ASA-CSSA-SSSA.

González-Delgado, A. M. & Shukla, M. K. (2014). Transport of nitrate and chloride in variably saturated porous media. *J. Irrig. Drain Eng.* 140(5) 04014006.

Gotovac, H., Cvetkovic, V., & Andricevic, R. (2009). Flow and travel time statistics in highly heterogeneous porous media. *Water Resources Res.* 45, W07402, DOI: 10.1029/2008WR007168.

Heeren, D. M., Fox, G. A., & Storm, D. E. (2014). Technical note: Berm method for quantification of infiltration at the plot scale in high conductivity soils. *J. of Hydrol. Eng.* 19(2), doi: 10.1061/(ASCE)HE.1943-5584.0000802.

Heeren, D. M., Fox, G. A., Storm, D. E., Haggard, B. E., Penn, C. J., & Halihan, T. July 21-24, 2013. Impact of Measurement Scale on Infiltration and Phosphorus Leaching in Ozark Floodplains. ASABE Annual International Meeting, Paper No. 1621213, Kansas City, Mo.

Heeren, D. M. (2012). Subsurface phosphorus transport and scale dependent phosphorus leaching in alluvial floodplains. PhD diss. Stillwater, Okla.: Oklahoma State University, Department of Biosystems and Agricultural Engineering.

Heeren, D. M., Fox, G. A., Miller, R. B., Storm, D. E., Mittelstet, A. R., Fox, A. K., Penn, C. J., & Halihan, T. (2011). Stage-dependent transient storage of phosphorus in alluvial floodplains. *Hydrol. Process.*, 25(20), 3230-3243.

Jarvis, N. J., Villholth, K. G., & Ulén, B. (1999). Modelling particle mobilization and leaching in macroporous soil. *European J. of Soil Sci.* 50(4): 621-632.

Lallemand-Barres, P. & Peaudecerf, P. (1978). Recherche des relations entre la valeur de la dispersivitie macroscopique d'un milieu aquifere, ses autres caracteristiques et les conditions de mesure, etude bibliographique. *Bulletin, Bureau de Recherches Geologiques et Miniéres*, 3/4: 277-287.

Larsson, M. H., Persson, K., Ulén, B., Lindsjö, A. & Jarvis, N. J. (2007). A dual porosity model to quantify phosphorus losses from macroporous soils. *Ecol. Modelling* 205: 123-134.

Lopez, C. B., Jewett, E. B., Dortch, Q., Walton, B. T., & Hudnell, H. K. (2008). Scientific Assessment of Freshwater Harmful Algal Blooms. Interagency Working Group on Harmful Algal Blooms, Hypoxia, and Human Health of the Joint Subcommittee on Ocean Science and Technology. Washington, DC.

McKeague, J., & Day, J. H. (1966). Dithionite and oxalate-extractable Fe and Al as aids in differentiating various classes of soils. *Canadian J. of Soil Sci.* 46: 13-22.

Miller, R. B., Heeren, D. M., Fox, G. A., Halihan, T., Storm, D. E., & Mittelstet, A. R. (2014). The hydraulic conductivity structure of gravel-dominated vadose zones within alluvial floodplains. *J. Hydrol.* 513: 229-240.

Miller, R. B. (2012). Hydrogeophysics of gravel-dominated alluvial floodplains in eastern Oklahoma. PhD diss. Stillwater, Okla.: Oklahoma State University, Department of Biosystems and Agricultural Engineering.

Mittelstet, A. R., Heeren, D. M., Storm, D. E., Fox, G. A., White, M. J., & Miller, R. B. (2011). Comparison of subsurface and surface runoff phosphorus transport rates in alluvial floodplains. *Agric. Ecosyst. Environ.* 141: 417-425.

MWPS (2001). Manure Storages. MWPS-18, Sec. 2. Ames, Iowa: Iowa State University.

Najm, M. R., Jabro, J. D., Iverson, W. M., Mohtar, R. H., & Evans, R. G. (2010). New method for the characterization of three-dimensional preferential flow paths in the field. *Water Resources Res.* 46, W02503, DOI:10.1029/2009WR008594.

OCES (2013). Using poultry litter as fertilizer. PSS-2246. Stillwater, Okla.: Oklahoma State University. Retrieved from http://poultrywaste.okstate.edu/Publications/files/pss-2246web.pdf.

Osborne, L. L., & Kovacic, D. A. (1993). Riparian vegetated buffer strips in water quality restoration and stream management. *Freshwater Biol.* 29(2): 243-258.

Pautler, M. C., & Sims, J. T. (2000). Relationships between soil test phosphorus, soluble phosphorus and phosphorus saturation in Delaware soils. *Soil Sci. Soc.of America Journal* 64: 765–773.

Radcliffe, D. E. & Šimůnek, J. (2010). *Soil physics with HYDRUS: Modeling and applications.* Boca Raton, Fla.: CRC.

Šimůnek, J., & van Genuchten, M. Th. (2008). Modeling nonequilibrium flow and transport processes using HYDRUS. *Vadose Zone J.* 7: 782–797, DOI: 10.2136/vzj2007.0074.

Šimůnek, J., Jarvis, N. J., van Genuchten, M. Th., & Gärdenäs, A. (2003). Review and comparison of models for describing non-equilibrium and preferential flow and transport in the vadose zone. *J. Hydrol.* 272: 14-35.